Supplementary Materials for

Contracting pore channels of a Magnesium-based metal-organic framework by decorating methyl groups for effective Xe/ Kr separation

Liangjun Li,*[a] Xu Zhang,[a, b] Wenli Xu,[a, b] Mengwei Guo,[a, b] Qingying Liu,[a, b] Fangru Li,[a, b] Tao Liu,[c, d] Tao Xing,[c, d] Zhi Li,[c, d] Mingqing Wang [c, d], Mingbo Wu,*[a, b, d]

[a] College of New Energy, China University of Petroleum (East China), Qingdao, 266580, China.

[b] College of Chemistry and Chemical Engineering, China University of Petroleum (East China), Qingdao, 266580, China.

[c] Research and Innovation Center of New Energy, Shandong Energy Group., Co. Ltd.,

[d] National Engineering Research Center of Coal Gasification and Coal-Based Advanced Materials.

Section 1: Materials and Methods

1.1 Materials

The metal salts, catalysts, and solvents are derived from commercial sources and used without further purification. The starting material: 2,3,5,6-tetramethyl-1,4-dibromobenzene, 3,5-dimethylphenylboronic acid ethyl ester was synthesized through a method reported in our previous literature. [1]

1.2 The synthesis of the ligand.

The ligand TMBDI was synthesized through the Suzuki coupling reaction between 2,3,5,6-tetramethyl-1,4-dibromobenzene with 3,5-dimethylphenylboronic acid ethyl ester, followed by hydrolysis to yield TMBDI. The synthetic route of ligand TMBDI is shown in Figure S1.

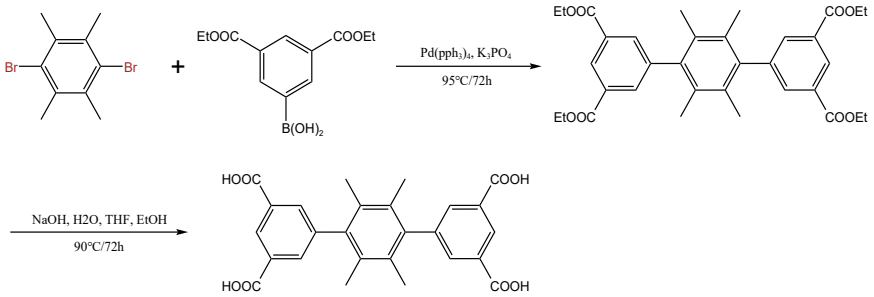

Figure S1 Schematic illustration of synthetic procedure of the ligand TMBDI

The synthesis of the ester intermediate of the TMBDI ligand: Place 300 ml of dioxane into a 500 ml Schlenk flask, and the flask was purged with nitrogen for a minimum of half an hour to eliminate any oxygen from the dioxane. In a separate 1000 ml three-necked flask, combine 2,3,5,6-tetramethyl-1,4-dibromobenzene (2.899g, 10 mmol) and 3,5-dimethylphenylboronic acid ethyl ester (6.385g, 24 mmol) alongside 21.0 g of anhydrous K_3PO_4. Introduce a stir bar to the three-necked flask and connect it to a Schlenk vacuum line. In a controlled environment, within a glovebox, carefully weigh out 0.5 g (0.43 mmol) of tetrakis(triphenylphosphine)palladium and transfer it into a Schlenk flask. Subsequently, transfer the catalyst from the Schlenk flask into the three-necked flask containing the reactants. Then, draw the dioxane into the three-necked flask. Switch on the magnetic stirrer, elevate the temperature of the reaction mixture to 90°C, and allow it to react at this temperature for a duration of 72 hours. Following the completion of the reaction, cool the mixture to room temperature.

Next, filter the reaction mixture and collect the filtrate. Subsequently, evaporate the filtrate to

remove the organic solvent. The resulting product is then purified via a silica gel column and subjected to column chromatography using an eluent composed of petroleum ether/ethyl acetate in a 10:1 ratio. This process yields a white powder-like product with an approximate yield of 80% based on the 2,3,5,6-tetramethyl-1,4-dibromobenzene used as the starting material.

The structure of the obtained intermediate was analyzed using nuclear magnetic resonance (1H NMR), and its 1H NMR spectrum is shown in Figure S2.

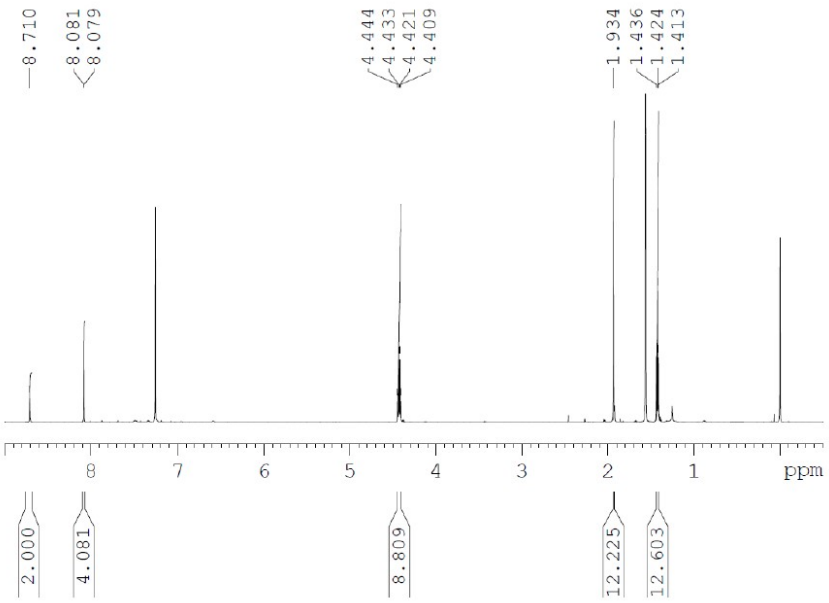

Figure S2 ^{1}H NMR Spectrum ($CDCl_3$-d1, 500 MHz) of the intermediate 2,3,5,6-tetramethylbenzene-1,4-di(3,5-diacetoxy)benzene

The ^{1}H NMR spectrum of the intermediate is as follows: 1H NMR ($CDCl_3$-d1, 500 MHz): 8.71 (s, 2H), 8.08 (d, 4H), 4.42 (q, 8H), 1.93 (s, 12H), 1.42 (t, 12H). The results of the spectrum are consistent with the expected structure of the intermediate, confirming the structure of the intermediate as 2,3,5,6-tetramethylbenzene-1,4-di(3,5-diacetoxy) benzene.

Hydrolysis of easter： Place 5.0 g of the ester intermediate into a three-necked flask, add 100 ml of ethanol and 100 ml of tetrahydrofuran, stir until dissolved, and then add 150 ml of 4M sodium hydroxide solution, stirring until dissolved. Heat the reaction mixture to reflux and let it react under reflux conditions for 12 hours, monitoring the progress of the reaction using thin-layer chromatography (TLC). After the reaction is complete, filter to remove any insoluble material, transfer the filtrate to a single-neck flask, and concentrate to remove the organic solvent. Then, add 100 ml of distilled water for dilution. Once the temperature has cooled to room temperature, slowly

add concentrated hydrochloric acid to adjust the pH of the reaction mixture to around 3, causing a significant amount of white precipitate to form. Filter the white precipitate, wash it three times with distilled water, and dry at 60℃ for 12 hours to obtain a ligand in the form of a white powder.

The structure of the obtained ligand was analyzed using nuclear magnetic resonance (1H NMR), and its 1H NMR spectrum is shown in Figure S3.

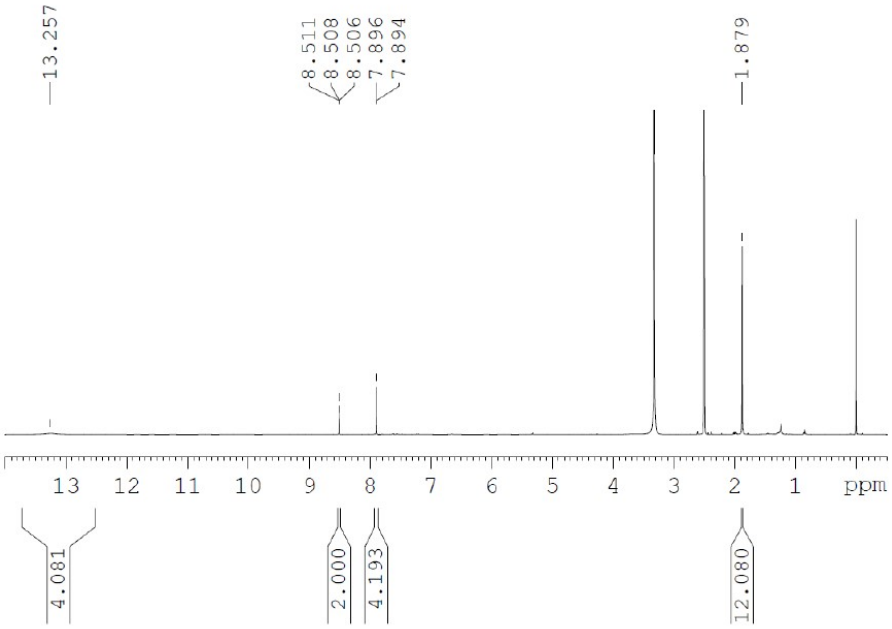

Figure S3 ^{1}H NMR Spectrum ($CDCl_3$-d1, 500 MHz) of the ligand TMBDI

The results of the 1H NMR spectrum are as follows: 1H NMR (DMSO-d6, 500 MHz): 13.257 (b, 4H), 8.51 (t, 2H), 7.89 (d, 4H), 1.88 (s, 6H). The NMR results are consistent with the expected structure of the ligand, confirming that the obtained substance is indeed the ligand TMBDI.

1.3 Synthesis of MOF material: Mg-TMBDI

Add ligand TMBDI (0.046 g, 0.1 mmol) and $Mg(NO_3)_2 \cdot 6H_2O$ (0.054 g, 0.2 mmol) into a 20 ml Teflon-line hydrothermal vessel. Follow this by adding 10 ml of N, N-dimethylacetamide (DMA) and 2 ml of water, and then incorporate 10 drops of concentrated nitric acid. Once the hydrothermal vessel is securely sealed, transfer it to a programmable temperature oven and gradually raise the temperature to 140°C, increasing by 40°C per hour. Maintain this temperature for a period of 72 hours. Subsequently, allow the vessel to cool to room temperature, at a controlled rate of 10°C per hour. To isolate the product, filter the mixture, yielding colorless needle-like crystals. Rinse these crystals with a solution of DMA and water, and then dry them at room temperature, ultimately obtaining white needle-like crystals.

1.4 Characterizations

1.4.1 Materials Characterization.

Powder X-ray diffraction (PXRD) measurements were conducted using a Cu Kα X-ray source in the 5 to 75° 2θ range (λ = 1.5406 Å) with a step size of 0.0167° on an X'Pert Pro X-ray diffractometer (Panalytical company, Netherlands). N_2 adsorption−desorption isotherms were acquired at 77 K using an Autosorb-iQ2 analyzer (Quantachrome, USA). Pore size distribution was determined from the desorption branch using the nonlocal density functional theory (NLDFT) method which is in-built with the software of the Autosorb-iQ2 analyzer. Additionally, thermogravimetric analyses (TGA) were performed in a nitrogen atmosphere, with temperatures ranging from ambient to 700°C and a heating rate of 10°C per minute , using a STA 449C instrument (Netzsch).

1.4.2 Singe-crystal X-ray diffraction

For single-crystal X-ray diffraction, larger and high-quality single crystals were selected for measurements. The diffraction data for Mg-TMBDI were gathered at 193 K using a Bruker SMART APEX CCD area detector, with graphite-monochromated Mo-Kα radiation (λ = 0.7173 Å). Structure determination involved direct methods and Fourier techniques through the utilization of the OLEX software package.[1] Hydrogen atom positions on the ligands were initially placed based on geometric considerations and later refined using a riding model. The unit cell volume exhibited a significant presence of disordered solvent molecules, which couldn't be accurately modeled as distinct atomic sites. To address this, we employed the PLATON/SQUEEZE[2] program to calculate the solvent's contribution to the diffraction data, resulting in a set of solvent-free diffraction intensities. All the crystallographic data and other details are listed in Table S1.

1.4.3 Gas sorption studies

Gas adsorption isotherms for Kr and Xe at various temperatures were determined utilizing a gravimetric method employing the magnetic suspension gravimetric gas adsorption analyzer (XEMIS, Hidden, UK). Prior to the gas sorption measurements, the Mg-TMBDI sample underwent a complete solvent exchange, with acetone being utilized as the solvent. Approximately 100 mg of the Mg-TMBDI sample was loaded onto the sample basket for the gas sorption assessments.

Prior to the gas adsorption measurements, the MOF was activated at 120°C under high vacuum conditions with a duration time of 8 hours. During the measurements, the gas uptake was determined

by weighing the sample adsorbed gas until reaching the equilibrium point, employing the magnetic suspension balance integrated into the apparatus. The adsorption temperature was precisely regulated using a computer-controlled water bath jacket, with a temperature control range within ±0.1 °C. The set pressure was meticulously maintained through computer-controlled pressure regulation integrated into the instrument.

1.4.4 Breakthrough experiments

Breakthrough experiments were conducted using a breakthrough analyzer (BSD-MAB, BeiShiDe Instrument Co., Ltd., Beijing, China). In this separation trial, we packed the sample of Mg-TMBDI (0.523 g) into a quartz tube with a 4 mm inner diameter. Prior to the breakthrough experiments, the sample inside the tube was activated by passing helium (20 ml/min) through it at 393 K for ten hours and then cooled to the measurement temperature of 298 K. Subsequently, a pre-mixed gas mixture of Kr and Xe (80/80, v/v) was used as the feed gas. The experiment was conducted at room temperature and pressure. The real-time composition and concentration at the outlet of the tube were detected by a mass-spectrometer.

1.4.5 GCMC simulations

The RASPA software[3] was employed to conduct computational Grand Canonical Monte Carlo (GCMC) simulations, analyzing the density distributions of gas molecules on Mg-TMBDI. Throughout the simulation, we treated the framework as immovable, and computed the non-bonded interactions between the gas molecules and Mg-TMBDI using the Lennard-Jones (L-J) potential. Cross-Lennard-Jones parameters were determined through the application of Lorentz-Berthelot mixing rules. For the gas molecules, the TraPPE forcefield was utilized, while the GeneralMOF forcefield was adopted for the Mg-TMBDI framework atoms. [4] Atomic partial charges of the Mg-TMBDI's host structure were incorporated into the DDEC method alongside quantitative calculations. The determination of pore structural parameters, including pore volumes, was carried out using the Zeo^{++} software package.[5]

Section 2: Tables and Figures

2.1 Crystal structures

The crystal structure parameters are presented in Table S1, and the packing mode presentation

of the crystal structure of Mg-TMBDI is shown in Figure S4.

Table S1 Crystallographic parameters of the Mg-TMBDI

Name	Mg-TMBDI
Molecular Formula	$C_{228}H_{200}O_{92}Mg_{16}$
Crystal System	Monoclinic
Space Group	*P2(1)/n*
Cell Parameters	***a***=16.781(2) Å, ***b***=21.602(3) Å, ***c***=22.461(3) Å
	α=90.000, ***β***=103.077(2), ***γ***=90.000
	V = 7931.2(18) Å^3
Z	4
Calculation of density	1.008 cm^3/g
F(000)	2504
Reflections collected/unique	7247/14520
Perspectives	1.32-25.4
R-value	R_1=0.0571, WR_2=0.1399

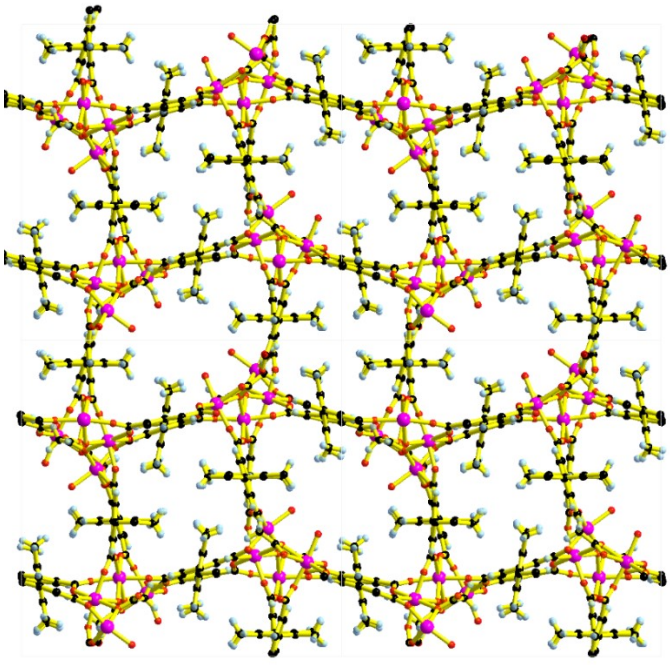

Figure S4 The packing mode presentation of the crystal structure of the Mg-TMBDI viewing from the *a* direction

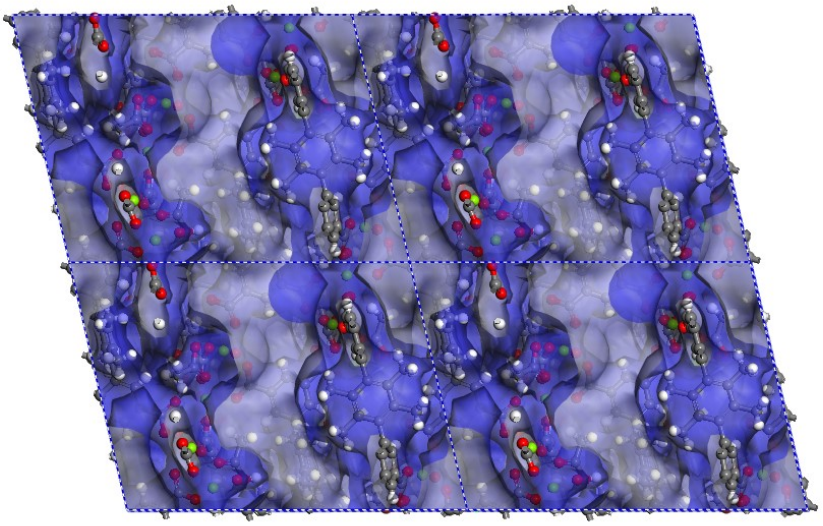

Figure S5 The inner pore surface of Mg-TMBDI

If the secondary structural unit is simplified to an 8-connected node, and the ligands are simplified to 4-connected nodes, its topological structure can be represented by the topological diagram shown in Figure S6.

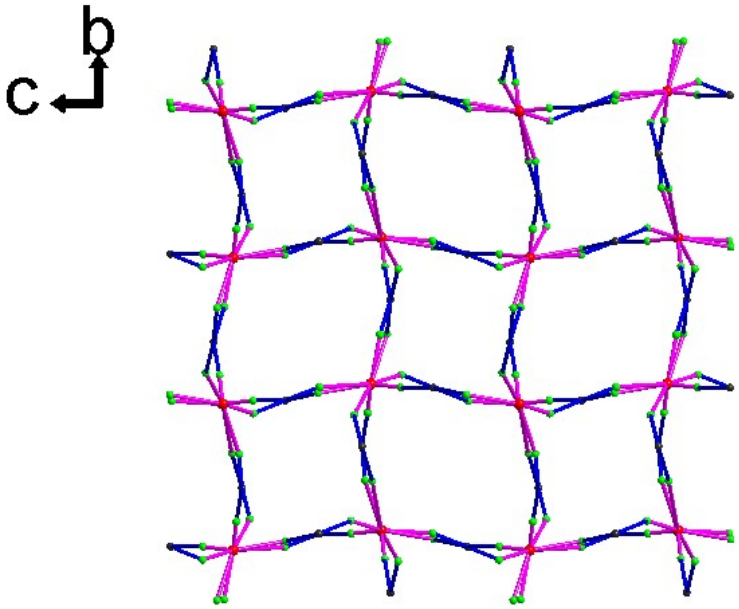

Figure S6 The topological network structure of the MOF material Mg-TMBDI

2.2 Powder X-ray diffraction patterns

To verify the structure of Mg-TMBDI, the powder X-ray diffraction patterns of Mg-TMBDI is collected (as shown in Figure S7). By comparing the PXRD (Powder X-ray Diffraction) pattern of the sample with the PXRD pattern obtained from single-crystal data fitting, it can be observed that the PXRD peak positions of the sample are in perfect agreement with those simulated, with no other impurity peaks detected.

To evaluate the water stability of the Mg-TMBDI. This MOF is subjected to a water-treatment process: the as-synthesized crystals of Mg-TMBDI is immersed in water for 24 hours. After water-treatment, the structure of obtained sample was evaluated through PXRD patterns and N_2 adsorption isotherm at 77 K.

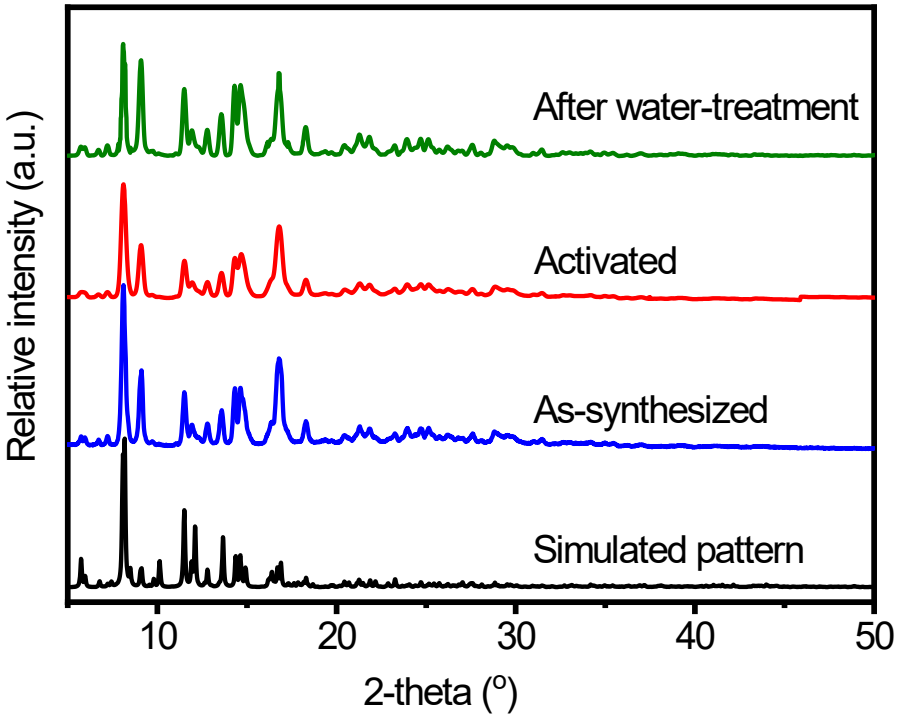

Figure S7 The PXRD pattern of MOFs at different status

2.3 N_2 isotherms

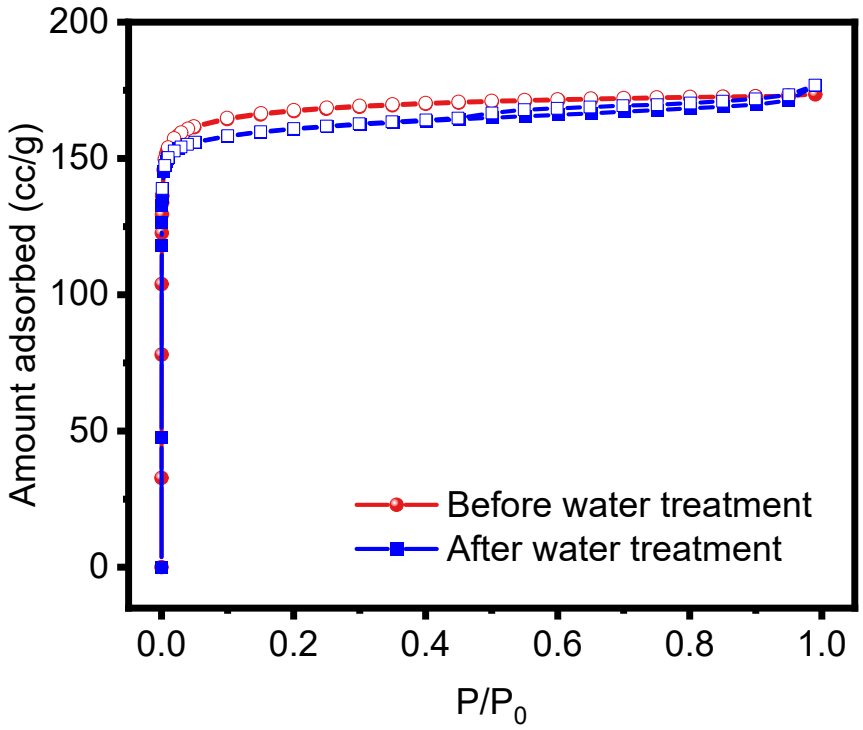

Figure S8 Comparison of N_2 isotherms of Mg-TMBDI before and after water treatment

2.4 Thermal gravimetric analysis

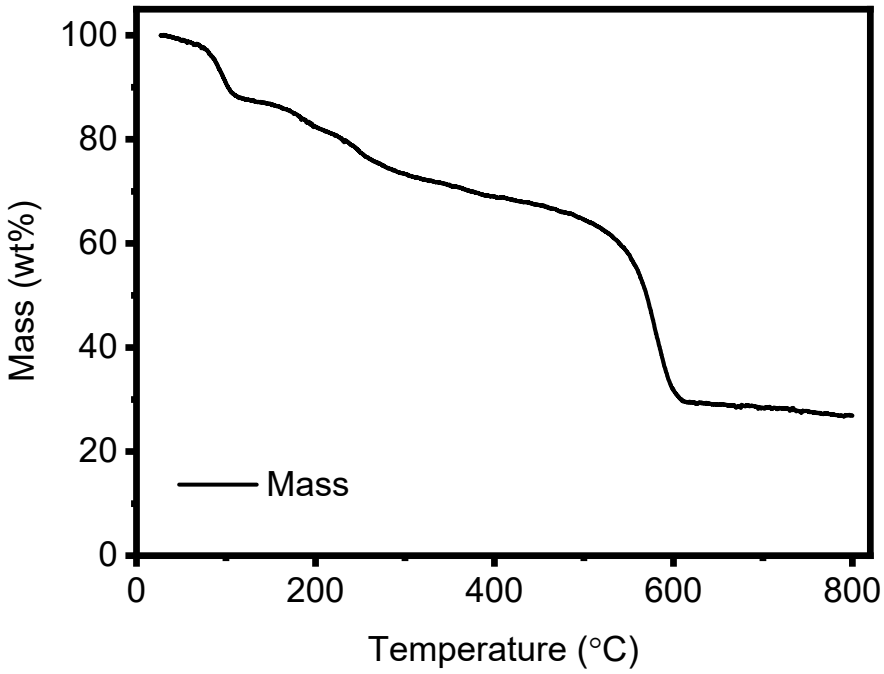

Figure S9 TGA curve of the Mg-TMBDI under N_2 atmosphere

2.5 Gas adsorption isotherms

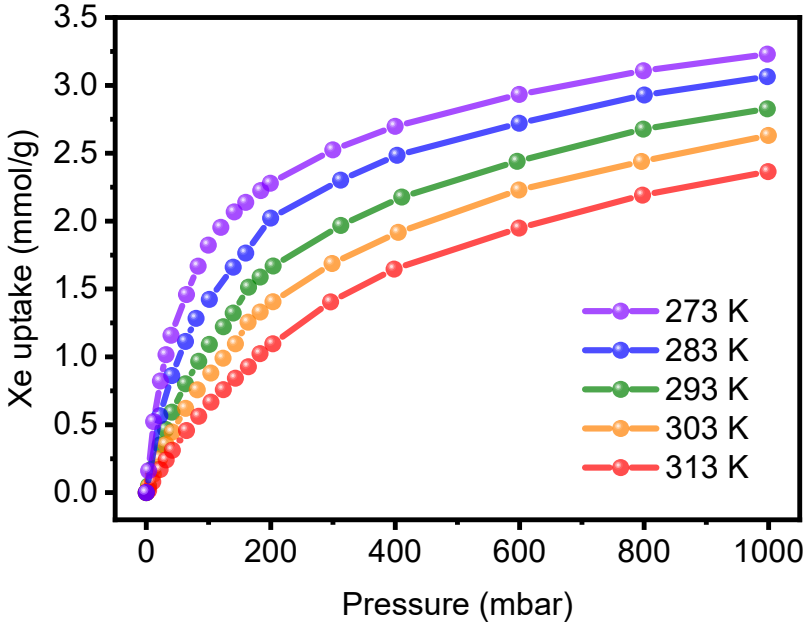

Figure S10 Xe adsorption isotherms at variable temperatures on Mg-TMBDI

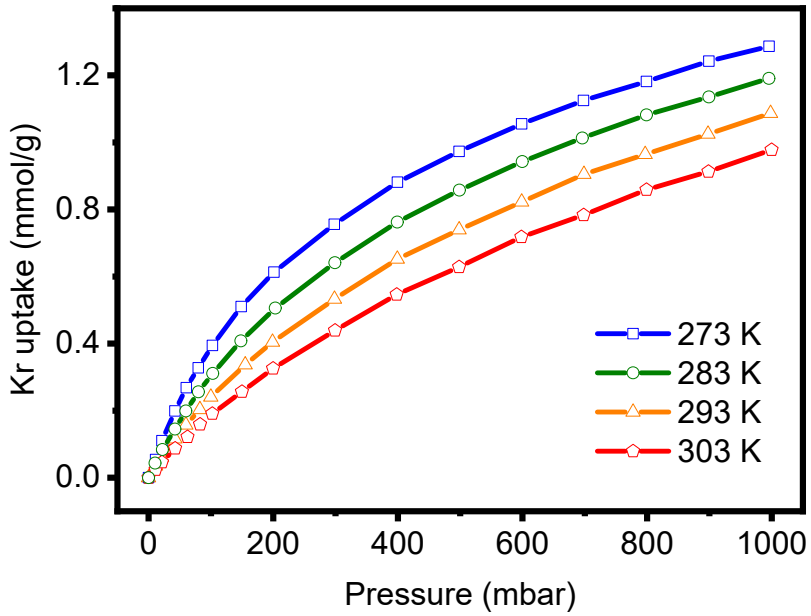

Figure S11 Kr adsorption isotherms at variable temperatures on Mg-TMBDI

2.6 Calculation of the isosteric adsorption enthalpy (Q_{st})

The isosteric adsorption enthalpy of Xe and Kr on Mg-TMBDI were calculated by the Clausius-Clapeyron equation:

$$\frac{Q_{st}}{R} = \frac{d(\ln P)}{d(1/T)}$$

The plot of lnP versus 1/T at specific loading were obtained from the Xe and Ke isotherms at variable temperatures. As shown in Figure S12 and S13, the term lnP exhibits an excellent linear relationship with (1/T), indicating the good reliability of the adsorption data. The slope of lnP versus 1/T were obtained from the linear fitting, and Q_{st} was calculated by using the above equation.

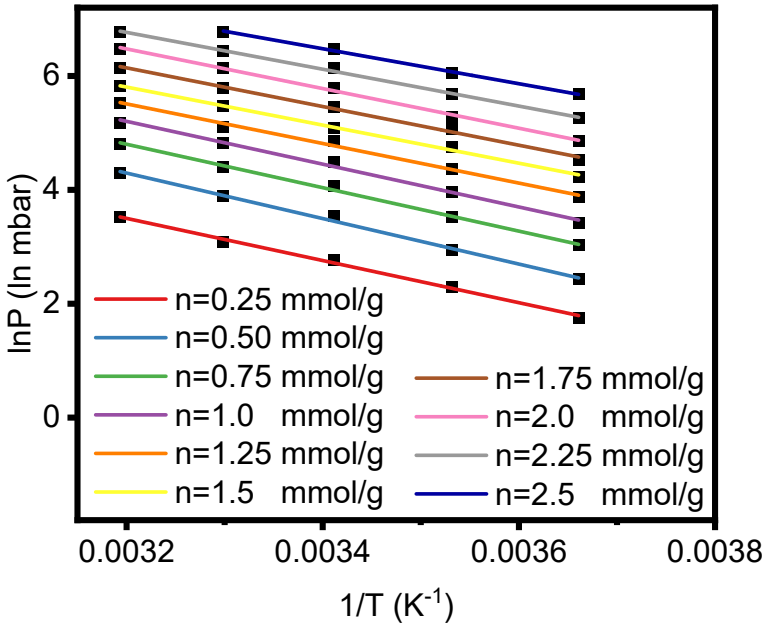

Figure S12 Linear fitting of lnP ~1/T at different loading for Xe adsorption on Mg-TMBDI

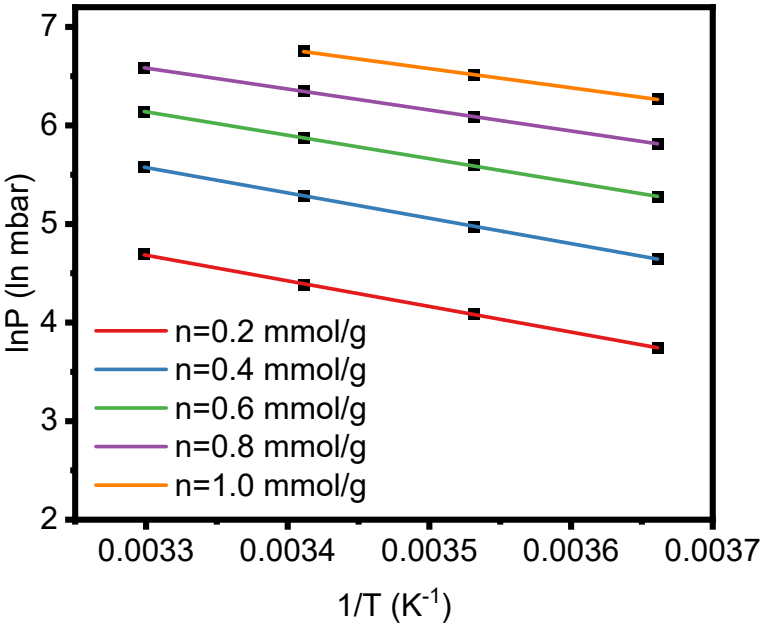

Figure S13 Linear fitting of lnP ~1/T at different loading for Kr adsorption on Mg-TMBDI

Table S2 Xe adsorption capacity and Xe/Kr selectivity of various materials at 298 K and 1.0 bar.

Adsorbents	Xe uptake (cm^3g^{-1}) 1.0 bar	IAST $S_{(Xe/Kr)}$	Xe Q_{st} KJ mol^{-1}	Ref
Mg-TMBDI	44.8	15	33.2	-
HIAM-401	43.8	13	32.7	[6]
TIFSIX-Cu-TPA	64.5	5.4	22.3	[7]
GeFSIX-Cu-TPA	61.2	5.3	21.7	[7]
NbOFFIVE-Cu-TPA	59.0	5.1	21.5	[7]
FJU-55	31.58	10	39.4	[8]
Al-CDC	54.88	10.7	40.6	[9]
JXNU-13-F	85.4	5.0	31.5	[10]
$Ni(NDC)(TED)_{0.5}$	27.1	12.9	28.1	[11]
Th-BPYDC-I	48.16	7.49	24	[12]
NU-1107-Ag(I)	20.6	13.4	28.7	[13]
NU-1106	38	10	-	[14]
UiO-66(Zr)	35.4	7.15	25	[15]
MIL-100(Fe)	25.54	5.59	20.9	[15]
MIL-101(Cr)	30.9	5.33	21.4	[15]
HKUST-1	70	8.5	26.9	[16]

References

[1] Dolomanov O. V., Bourhis L. J., Gildea R. J., Howard J. A., Puschmann H. OLEX2: a complete structure solution, refinement and analysis program [J]. Journal of Applied Crystallography, 2009, 42(2): 339-341.

[2] Spek A. Single-crystal structure validation with the program PLATON [J]. Journal of Applied Crystallography, 2003, 36(1): 7-13.

[3] Dubbeldam D., Calero S., Ellis D. E., Snurr R. Q. RASPA: molecular simulation software for adsorption and diffusion in flexible nanoporous materials [J]. Molecular Simulation, 2016,

42(2): 81-101.

[4] Li Z., Liao F., Jiang F., Liu B., Ban S., Chen G., Sun C., Xiao P., Sun Y. Capture of H2S and SO2 from trace sulfur containing gas mixture by functionalized UiO-66 (Zr) materials: A molecular simulation study [J]. Fluid Phase Equilibrium, 2016, 427: 259-267.

[5] Willems T. F., Rycroft C. H., Kazi M., Meza J. C., Haranczyk M. Algorithms and tools for high-throughput geometry-based analysis of crystalline porous materials [J]. Microporous and Mesoporous Materials, 2012, 149(1): 134-141.

[6] Guo F-A, Zhou K, Liu J, Li X, Wang H: A microporous Zr6@Zr-MOF for the separation of Xe and Kr. Dalton Transactions 2022, 51:10856-10859.

[7] Li J, Wang L, Chen Y, Gu Z, Jiang T, Luan B, Krishna R, Zhang Y: Efficient Xe/Kr separation in fluorinated pillar-caged metal-organic frameworks. Microporous and Mesoporous Materials 2023, 357.

[8] Gong L, Liu Y, Ren J, Al-Enizi AM, Nafady A, Ye Y, Bao Z, Ma S: Utilization of cationic microporous metal-organic framework for efficient Xe/Kr separation. Nano Research 2022, 15:7559-7564.

[9] Zhu Z, Li B, Liu X, Zhang P, Chen S, Deng Q, Zeng Z, Wang J, Deng S: Efficient Xe/Kr separation on two Metal-Organic frameworks with distinct pore shapes. Separation and Purification Technology 2021, 274.

[10] Wang J-Z, Fu X-P, Liu Q-Y, Chen L, Xu L-P, Wang Y-L: Dinuclear Nickel–Oxygen Cluster-Based Metal–Organic Frameworks with Octahedral Cages for Efficient Xe/Kr Separation. Inorganic Chemistry 2022, 61:5737-5743.

[11] Zhao Z, Xiong H, Peng Y, Liu X, Wang P, Liu J, Deng Z, Chen S, Chen J, Zhou Z, et al: Pore environment modulation of metal-organic frameworks enables efficient adsorptive separation of Xe/Kr. Separation and Purification Technology 2023, 325.

[12] Mi P, Chen L, Li X, Wang X, Li G, Cheng L, Lu J, Zhang H, Wang Y, Wang S: Enhanced Xe/Kr separation via the pore size confinement effect of a microporous thorium-based metal–organic framework. Dalton Transactions 2022, 51:15233-15238.

[13] Gong W, Xie Y, Wang X, Kirlikovali KO, Idrees KB, Sha F, Xie H, Liu Y, Chen B, Cui Y, Farha OK: Programmed Polarizability Engineering in a Cyclen-Based Cubic Zr(IV) Metal–Organic Framework to Boost Xe/Kr Separation. Journal of the American Chemical Society 2023,

145:2679-2689.

[14] Maldonado RR, Zhang X, Hanna S, Gong X, Gianneschi NC, Hupp JT, Farha OK: Squeezing the box: isoreticular contraction of pyrene-based linker in a Zr-based metal–organic framework for Xe/Kr separation. Dalton Transactions 2020, 49:6553-6556.

[15] Lee S-J, Yoon T-U, Kim A-R, Kim S-Y, Cho K-H, Hwang YK, Yeon J-W, Bae Y-S: Adsorptive separation of xenon/krypton mixtures using a zirconium-based metal-organic framework with high hydrothermal and radioactive stabilities. Journal of Hazardous Materials 2016, 320:513-520.

[16] Soleimani Dorcheh A, Denysenko D, Volkmer D, Donner W, Hirscher M: Noble gases and microporous frameworks; from interaction to application. Microporous and Mesoporous Materials 2012, 162:64-68.